Food Control 159 (2024) 110284

Contents lists available at ScienceDirect

Food Control

journal homepage: www.elsevier.com/locate/foodcont

Combination of spectral and textural features of hyperspectral imaging for the authentication of the diet supplied to fattening cattle

Sara León-Ecay [a], Kizkitza Insausti [a], Silvia Arazuri [b], Irantzu Goenaga [a,c], Ainara López-Maestresalas [b,*]

[a] Institute on Innovation and Sustainable Development in Food Chain (IS-FOOD), Department of Agricultural Engineering, Biotechnology and Food, ETSIAB, Universidad Pública de Navarra, Campus de Arrosadia, 31006, Pamplona, Spain
[b] Institute on Innovation and Sustainable Development in Food Chain (IS-FOOD), Department of Engineering, ETSIAB, Universidad Pública de Navarra, Campus de Arrosadia, 31006, Pamplona, Spain
[c] Tratamiento Subproductos Agroalimentarios, S.L. (TRASA), Camino San Juan s/n, 31320, Milagro, Spain

ARTICLE INFO

Keywords:
Meat quality
Animal feeding
Hyperspectral imaging
Feature combination
Machine learning

ABSTRACT

This study explored the potential of hyperspectral imaging in the near infrared region (NIR-HSI) as a non-destructive and rapid tool to discriminate among two beef fattening diets. For that purpose, a feeding trial was carried out with a total of 24 purebred Pirenaica calves. Twelve of them were fed barley and straw (BS) while 11 animals were finished on vegetable by-products (VBPR). When comparing the reference measurements of the meat coming from those animals, only the total collagen ratio expressed the feeding effect (p-value<0.05). To undertake the authentication procedure, two discrimination approaches were run: partial least squares discriminant analysis (PLS-DA) and radial basis function-support vector machine (RBF-SVM). To precisely extract spectral and textural information from the lean portion of the meat steaks, various techniques were executed, such as principal component (PC) images, competitive adaptive reweighted sampling (CARS) for selecting optimal wavelengths, and gray-level-co-occurrence matrix (GLCM). After hyperspectral imaging and the combination of their own texture features, samples were classified according to feeding diet with an overall accuracy of 72.92% for PLS-DA and 80.56% for RBF-SVM. So, the potential of using HSI technology to authenticate the meat obtained from beef supplied a diet based on circular economy techniques was made in evidence.

1. Introduction

The manufacturing of enough protein to satisfy humans' both structural and energy metabolism requirements, considering in turn a world population growing rate of around 1.13% per year (from 7.4 billion in 2016 to 8.1 billion in 2025), and the unstable economic situation, powers the competitiveness between food production for animals and human food (Tripathi et al., 2019). Besides, 40% of the total quota associated to arable land is destined for livestock feed, increasing the stress on the current food system (Godfray et al., 2018, p. 361; Sandström et al., 2022). It is necessary to booster the sustainability of the food chain and ensure food security, this being understood as an access to a consistent, sufficient, safe, and nutritious food for the entire population (Attrey, 2017). Hence, the transition to a circular system is reported as the alternative economic model (Despoudi et al., 2021; Fassio et al., 2022).

The need to guarantee the sustainability of food production leads to a new search for Circular Economy (CE) and valorization techniques to make the best use of natural resources, moving towards a carbon-neutral future. According to Wadhwa and Bakshi (2013) about 50% of all fruits and vegetables in the European Union (EU) go to waste during agricultural production, processing, distribution and, consumption. For instance, only in the EU vegetable sector, from the 900 Mt produced, around 300 Mt were discarded, comprising the 24% of the total food waste and a 21% of the carbon footprint (Espinosa-Alonso et al., 2020).

In the field of animal production, alternative novel feed resources for ruminants to reduce feed/food competition, enhance circularity, and reduce the environmental footprint are being introduced (Silva et al., 2016; Tzamaloukas et al., 2021). As determined in The Dublin Declaration of Scientists on the Societal Role of Livestock (2023), ruminants can give a second life to the inedible biomass by humans that is mainly generated during the process of obtaining food for human consumption. This, linked to the high amount of vegetable by-products (VBPR)

* Corresponding author.
E-mail address: ainara.lopez@unavarra.es (A. López-Maestresalas).

https://doi.org/10.1016/j.foodcont.2024.110284
Received 11 September 2023; Received in revised form 23 November 2023; Accepted 1 January 2024
Available online 2 January 2024

Abbreviations

NIR-HSI	hyperspectral imaging in the near infrared region
BS	barley and straw
VBPR	vegetable by-products
PLS-DA	partial least squares discriminant analysis
RBF-SVM	radial basis function-support vector machine
PC	principal component
CARS	competitive adaptive reweighted sampling
GLCM	gray-level-co-occurrence matrix
CE	circular economy
EU	European union
UV/Vis	ultraviolet–visible
NIR	near infrared
MIR	mid infrared
OW	optimal wavelengths
PGI	protected geographical indication
LDL	Longissimus dorsi lumborum
WBSF	Warner Bratzler Shear Force
SRS	spectral reduction strategies
ROI	region of interest
MC	monte carlo
RMSECV	root mean square error of cross validation
PLS	partial least squares
TF	texture features
CON	contrast
COR	correlation
ENE	energy
HOM	homogeneity
ENT	entropy
ASM	Angular Second Moment
PCC	Pearson correlation coefficient
ANOVA	analysis of variance
MP	mathematical preprocess
SM	smoothing
SNV	standard normal variate
MSC	multiplicative scatter correction
MC	mean center
SG	Savitzky-Golay
LV	latent variable
CV	cross validation
CC	correctly classified
TP	true positives
TN	true negatives
FP	false positives
FN	false negatives
IMF	intramuscular fat
PCA	principal component analysis
MS	mean spectra

generated daily by the industry, presents an opportunity for ruminants to take advantage of them.

Even though there is a great difference within the parts of the same by-product, they are considered as a valuable source of sugars, fiber, lipids, organic acids, flavonoids, vitamins, and minerals (Rao et al., 2021). Also, vegetable by-products stand out by their recognized antioxidant and antimicrobial properties making them really interesting for animal feeding (Bharat Helkar & Sahoo, 2016; Nardella et al., 2022).

Notwithstanding, there is no point in providing animals with a sustainable diet if the meat preparations are mislabeled so that end consumers cannot tell the difference at first glance. Ensuring the safety and quality of them is crucial to maintain the competitiveness of the meat sector able to market a value-added and environmentally sustainable product. The development of rapid, friendly, and non-invasive measurement methods as an alternative for both the prediction of meat quality and the authentication of meat products is under continuous study (Prieto et al., 2018). Thus, innovations and technological advancements related to quality assessment and authentication, throughout UV/Vis, Raman, NIR and MIR, among other technologies, have become a priority in recent years (Barragán et al., 2021; Basantia et al., 2019; Jia et al., 2022; Katemala et al., 2021; Malavi et al., 2023). Hyperspectral imaging (HSI) is said to revolutionize the meat industry as it will have a positive impact on reducing meat fraud, waste, and recalls (Feng & Sun, 2012; Jia et al., 2022; Ma et al., 2019).

Due to the complexity of the signal profiles obtained from the spectroscopic instruments, multivariate analysis plays a crucial role, as it is an extremely powerful tool for data processing (Biancolillo et al., 2020). In this respect, chemometric models can either have as input the spectral information provided by the hyperspectral images or the combination of this data with the textural characteristics of the images themselves. One of the major applications of the second approach in meat products and fresh meat has been in the study of lamb and pork (Kucha et al., 2022; X. Li et al., 2023; Robert et al., 2023; Wan et al., 2023). But other meats have also been studied in recent years. Thus, Xiong et al. (2015) differentiated among free-range and broiler chicken using HSI with a RBF-SVM model obtaining a CC rate of 93.33% for the test set while Weng et al. (2021) authenticated mutton geographical origin and breed using spectra of effective wavelengths and effective variables of textural features with an accuracy of 99.07% for the train set through SVM. Considering beef meat, this approach has been applied to predict meat quality traits (Liu et al., 2014; Yang et al., 2017) while a smaller number of studies have been conducted for classification. Thus, to go one step forward on the state-of-the-art, the aim of this study was to authenticate the diet (barley and straw (BS) vs. vegetable by-products (VBPR)) supplied to fattening calves by combination of spectral and texture features of hyperspectral imaging. As far as we are concerned, no studies have been published on the use of this approach to differentiate meat from fattening calves finished with two different diets.

Therefore, the specific objectives of this study were to: (1) discriminate between meat cuts from fattening calves finished with a conventional ration vs. a vegetable by-product diet using near-infrared-HSI; (2) identify optimal wavelengths (OWs) by the competitive adaptive reweighted sampling (CARS) algorithm; and, (3) build classification models by combining spectral and textural data using partial least squares-discriminant analysis (PLS-DA) and radial basis function-support vector machine (RBF-SVM).

2. Materials and methods

2.1. Experimental design: animals and diets

Twenty-three entire young bulls reared under the Protected Geographical Indication (PGI) "Ternera de Navarra" were used in this study. They were handled following the experimental procedures for handling cattle exposed on the European Directive 2010/63/EU (EEC, 2010) regulated in Spain by the Royal Degree 348/2000 (Ministerio de Agricultura, Pesca y Alimentación, 2000). Besides, the animal husbandry guidelines proposed by the PGI were followed. Twelve animals were supplied a diet based on 90% barley and 10% straw (BS, conventional diet), whereas the remaining 11 animals were supplied a diet based on vegetable by-products (VBPR), composed by 53.08% concentrated feed, 37.4% of vegetable by-products, 5.45% beet pulp and 4.07% straw. More information about the diets supplied can be found in Goenaga et al. (2023). Both diets, together with water, were provided

ad-libitum.

The fattening period lasted for 139.73 ± 18.54 days. Once the standard fattening period for the PGI established in the EEC 1483/2004 (EEC, 2004) elapsed, from 6 to 13 months of age, animals were transported from the industrial farm located in Azoz, Navarra (Spain), to the EU-commercial abattoir AlmaMeat S.L.U. located in Salinas de Pamplona, Navarra (Spain) the day before slaughter, in compliance with the current European Community of Animal Welfare in transport. They were stunned with a captive bolt and subsequently slaughtered and dressed according to the specifications outlined in the EEC 93/119/1993 (EEC, 1993). Animals were slaughtered for productive purposes in 4 batches from March to May 2022.

Then, 23 steaks (25 mm-thick ± 0.2 mm) from the *Longissimus dorsi lumborum* (LDL) muscle were taken from the left side of each carcass of the 23 purebred Pirenaica calves. The cuts were then cooled, vacuum packaged, and aged for 7 days into a cooler (Kide, Berritua, Bizkaia, Spain) at 5 °C and 80% of relative humidity, at the post-harvest laboratory of the School of Agricultural Engineering and Bioscience of the Universidad Pública de Navarra located in Pamplona, Spain.

2.2. Reference measurements

Once the aging days were over, LDL meat samples analysis was performed. After 1 h of blooming at room temperature, the CIE Lab coordinates L*, a*, b*, C* and h* of the surface of each steak were measured at five different points using a Minolta CR-400 (illuminate: D65) colorimeter.

Texture was assessed complying with the specifications proposed by the AMSA guideline (American Meat Science Association, 2016, pp. 1–106). Succinctly, the samples were cooked on a water bath until the internal temperature reached 70 °C, controlled by a probe Digitron (Hereford, UK) model 3246 thermocouples. To register the maximum Warner Bratzler Shear Force (WBSF), in newtons (N), an IBM-compatible Foxen computer, equipped with the software "Texture Expert" version 1.22 to Windows (Stable Micro Systems, Surrey, UK), was employed connected to a TA-XT2i Stable Micro Systems texturometer. System force calibration was carried out with a 5 kg weight. Six to eight replicates of 1 cm^2 and at least 30 mm long were analyzed per sample by a stainless-steel Warner Bratzler V Slot Blade probe, with a thickness of 1.06 mm containing a vee-shaped (60° angle) cutting edge. The experiment was computed with a maximum capacity of 30 kg at a speed of 1.70 mm/s, in compliance with the specifications of the method proposed by Novaković and Tomašević (2017).

Crude fat was appraised in duplicate by Soxhlet using diethyl ether as solvent after a previous acid hydrolysis, following the ISO 1443:1973 while Kjeldahl method specified in the ISO 937:1978 was performed, also in duplicate, to ascertain crude protein. Total collagen was quantified in double with the methodology proposed by Bonnet and Kopp (1992).

2.3. Hyperspectral imaging acquisition and processing

2.3.1. Hyperspectral system

The 23 initial samples were scanned from both sides, that is, 46 hyperspectral images (23 steaks × 2 sides) were acquired, which were subsequently treated completely independently of each other.

The setup used to record the images consisted of 4 main elements: (a) an illumination module comprised of 4 halogen lamps of 28 W (W), (b) a carrier plate for moving the steaks, (c) a hyperspectral camera and, (d) a computer endowed with two software programs: Xeneth 2.5. and ACT Controller for camera and transportation plate handle, respectively. The hyperspectral camera used (Xenics, Model Xeva-1.7- 320, Leuven, Belgium), with a 320 x 256 pixel resolution, was coupled to an ImSpector N17E spectrograph (Specim, Spectral Imaging Ltd., Oulu, Finland) both sensitive in the 900–1700 nm spectral range, and to a lens (Xenics, Model OPT-000107, SWIR 16 mm f/1.4, Leuven, Belgium) with a focal length of 16 mm.

2.3.2. Image acquisition and normalization

The mentioned device is a line scanning or pushbroom system that records a line image of the samples each time. Thus, to capture the data from the whole steak the samples must be moved under the field of view of the camera. The object-distance was set up to 40 cm height and the platform speed reached 7 mm/s. The integration time was set at 2000μs. Due to this common configuration for all the samples, the three-dimensional (3D) images presented the following size: 320 columns (0.75mm/pixel), 256λ (every 3.14 nm), and a variable number of rows according to the steak size. To remove surface moisture, all samples were wiped off by paper towels before image acquisition.

To guarantee the representability and reproducibility of the study, it is required to radiometrically correct the raw images (I_{raw}) to avoid spectral nonuniformities (Shaikh et al., 2021). For that purpose, all I_{raw} were normalized by both the dark and white references. Dark reference (I_{black}) was taken with the lens covered, while the white reference (I_{white}) was recorded using a certified *Spectralon* tile (Standard 99%, Labsphere) with the following dimensions: 600 x 50 × 10 mm. Thus, each corrected hypercube (I_c) was obtained by applying Eq. (1).

$$I_c = \frac{I_{raw} - I_{black}}{I_{white} - I_{black}} \quad \text{Eq.1}$$

Before starting with data processing, the 3D normalized images ((a) rows, (b) columns, (c) wavelengths) must be unfolded with the aim of obtaining a computationally manageable two-dimensional matrix ((a) rows x columns, (b) wavelengths). Once this essential step is completed, it is possible to proceed with image processing applying spectral reduction strategies (SRS).

2.4. Data volume reduction strategies

2.4.1. Image segmentation and extraction of the region of interest (ROI)

Hyperspectral images include the background, the lean portion of the beef steaks, the fat flecks, and the connective tissue placed around. Regarding the former, it is characterized by being a highly noisy part able to diffuse the results. In the absence of image processing, both the mentioned noisy spectra and the non-lean fraction can negatively distort the further classification due to the obvious differences in several regions (ElMasry et al., 2011). Hence, a region of interest (ROI), which gathers a reduced number of pixels, should be selected to provide enough information to represent the entire steak.

In this study, two ROIs were selected and independently modelled. First, the whole lean portion of the samples was used for analyses and then, in a second step, a random selection of 25% of the pixels contained in the lean portion of each steak were also used for modelling. Considering the first one, a mask was used to remove both the background and the non-lean section of the steaks by applying the *K-means* clustering portioning method. The spectral data was shared out into $k = 3$ mutually exclusive clusters, to subsequently obtain the index of the cluster to which it assigns each observation. Afterwards, the isolation of the lean portion was achieved. For the second ROI, the 25% of the total pixels extracted with the lean portion mask were secluded in a random way.

To guarantee the reliability of the models, in both methodologies, samples were randomly split into train and test sets with a ratio of 78:22, respectively, ensuring that all pixels of the same steak were kept in the assigned matrix. Thus, after the isolation of the lean portion X matrices of the following dimensions: 837,856 x 207 and 233,713 x 207 were obtained for train and test, respectively. On the other hand, once the 25% of the total pixels were randomly extracted from the lean portion mask, the X dataset was reduced to 209,468 x 207 for train and 58,430 x 207 for test.

2.4.2. Extraction of efficient spectral wavelengths

The band range of the original hyperspectral images span from 900

to 1700 nm. The first 49 wavelengths were eliminated due to low signal-to-noise ratio. Although these wavelengths were removed to avoid data tempering and to reduce test time, problems associated to high dimensionality and redundancy among the variables, that may further diminish the precision of the multivariate models, could still be found as pointed out by Wan et al. (2023).

To identify a subset of variables that represented the highest variability of the entire dataset, the competitive adaptive reweighted sampling algorithm was proposed. CARS, based on the principle of "survival of the fittest" from Darwin's evolution theory, has been widely applied as a feature selection algorithm when considering food samples. It is characterized by the selection of N subsets of wavelengths from Monte Carlo (MC) sampling runs to afterwards evaluate the importance of each wavelength, using as index the regression coefficients of a PLS model (Li et al., 2009). Finally, the subsets with the lowest root mean square error of cross validation (RMSECV) are selected to continue with the study. The parameters used in the set up were as follows: 10-fold cross validations, 30 iterations of CARS and a maximum of 7 PLS components, so the number of variables were reduced from the initial 207 to 150.

2.4.3. Principal Component Analysis (PCA)

For feature reduction purposes, while retaining most of the variability of the dataset, extraction of principal component (PC) images from the spectral variables was carried out. As an input for the further classification models, only the top PCs were selected considering the optimal ones in cross validation, this is, the PCs that recorded the lowest RMSECV, being in this case, the first three (X_{train}: 837,856 x 3).

2.4.4. Extraction of textural data

Statistical and structural approaches to image texture have been widely studied as years pass by. Also, it has moved from first order statistics measures based only on the intensity of individual pixel values to second order measures which are characterized by dealing with a pair of pixels in the image (Aouat et al., 2021). It was Hawlick (1979) who first introduced the concept of gray-level co-occurrence matrix (GLCM), becoming one of the most popular statistical texture analysis methods. Its application has been such since the biochemical and biophysical characteristics of the samples can be expressed in the texture of hyperspectral images (Wu et al., 2023). Its basis lies in calculating how often a pixel with gray-level (grayscale intensity) value *i* occurs horizontally adjacent to a pixel with gray-level value *j* (Haralick et al., 1973). From the matrix, statistical texture features (TFs) can be extracted, being able to capture unique characteristics of the product itself.

To this end, in this study, five TFs including contrast (CON) (Eq. (2)), correlation (COR) (Eq. (3)), energy (ENE) (Eq. (4)), homogeneity (HOM) (Eq. (5)), and entropy (ENT) (Eq. (6)) were computed from each ROI throughout a GLCM with different moving directions ($\theta = 0°$, $45°$, $90°$, and $135°$) and distance (D) = 1 to subsequently calculate the average value of the 4 directions.

According to Zayed and Elnemr (2015) two of the attributes are, typically, indirectly proportional since CON represents local variations by calculating the sum of squares among reference and neighbor pixels (Park et al., 2023), whereas HOM measures how close the distribution of the elements is to the diagonal of the GLMC matrix (Reis et al., 2018). As for Zayed and Elnemr (2015) COR describes the linear dependency of gray-level values in the co-occurrence matrix meanwhile ENE is also known as Angular Second Moment (ASM) as it measures the uniformity of the gray-levels. In the assumption of similar pixels, ENE value will increase. Finally, ENT is theoretically inverse to ENE (Gade & Vyavahare, 2018).

To calculate the mentioned TFs, the following equations should be applied:.

$$\text{Contrast} = \sum_{i=1}^{N}\sum_{i=1}^{N}(i\text{-}j)^2 P(i,j) \quad \text{Eq.2}$$

$$\text{Correlation} = \frac{\sum_{i=1}^{N}\sum_{i=1}^{N}(ij)P(i,j)\text{-}\mu_i\mu_j}{\sigma_i\sigma_j} \quad \text{Eq.3}$$

$$\text{Energy} = \sum_{i=1}^{N}\sum_{i=1}^{N}P(i,j)^2 \quad \text{Eq.4}$$

$$\text{Homogeneity} = \sum_{i=1}^{N}\sum_{i=1}^{N}\frac{P(i,j)}{1+(i\text{-}j)^2} \quad \text{Eq.5}$$

$$\text{Entropy} = \sum_{i=1}^{N}\sum_{i=1}^{N}P(i,j)\lg(P(i,j)) \quad \text{Eq.6}$$

where μ and σ are the average and the standard deviation of the data in the GLCM, respectively.

As each band is associated to a gray scale image from each hyperspectral image, 4140 TFs were obtained (4 directions x 5 TFs x 207 wavelengths) from the GLCM. To ease the processing of the data and overcome computational limitations due to the high amount of data generated, a Pearson correlation coefficient (PCC) was calculated to finally select the most efficient TFs. The PCC was calculated using Eq. (7) (Fisher, 1992), through which it is possible to study the relationship between two random variables.

$$\rho(A,B) = \frac{1}{N\text{-}1}\sum_{i=1}^{N}\left(\frac{A_i\text{-}\mu_A}{\sigma_A}\right)\left(\frac{B_i\text{-}\mu_B}{\sigma_B}\right) \quad \text{Eq.7}$$

where μ_A and σ_A correspond to the mean and standard deviation of the A variable, respectively, while μ_B and σ_B correspond to the mean and standard deviation of B, respectively.

The entire procedure was calculated using MATLAB R2020a (The Mathworks Inc., Natick, MA, USA) in addition to complementary own codes.

2.5. Statistical analysis

2.5.1. Analysis of the variance

Beef meat quality statistics were accomplished with the software SPSS Statistics (IBM Corp. Released 2021. IBM SPSS Statistics for Windows, Version 28.0.1.1. Armonk, NY: IBM Corp). To screen for variations among quality parameters through traditional instrumental measures, an Analysis of Variance was conducted (ANOVA) between groups being diet the fix effect.

2.5.2. Data pre-processing and chemometric analysis

Spectral data, in addition to the chemical information, contain irrelevant artifacts as electrical noise and stray light (Bian, 2022). To keep only useful details before starting with chemometric techniques, it is necessary to mathematically preprocess (MP) the data. Among the most common pre-processing methods, the following are becoming more prominent: (a) spectral smoothing techniques (SM), (b) standard normal variate (SNV), (c) multiplicative scatter correction (MSC), (d) mean center (MC), and (e) first (1st der) and second order (2nd der) derivatives.

To isolate spectral features that could be cryptic by noise, a Savitzky-Golay (SG) smoothing method of a 2-order polynomial and a 15-point window was applied. Its basis lies on fitting successive subsets of adjacent scattered data points employing linear least squares (Selver et al., 2018), with the objective of obtaining a high signal-to-noise ratio retaining the original shape of the signal (Acharya et al., 2016). Sifting to the scatter correction category, SNV was applied to minimize surface scattering, minimize optical path changes, and eliminate the influence of the particle size meanwhile MSC eliminated the unwanted effect of spread out from both particle distribution and size (Bian, 2022). Finally, derivatives were used for baseline correction and resolution enhancement. The spectral data were subjected to the above-mentioned pre--processing techniques, either individually or in combination.

Two types of discrimination approaches were performed. The first, PLS-DA, is a supervised analysis and linear algorithm whereas the second, RBF-SVM, is a non-linear algorithm. Both were computed in MATLAB R2020a (The MathWorks, Natick, MA, USA) while the former was run also by the software PLS_Toolbox version 9.0 (Eigenvector Research Inc., Wenatchee, WA, USA).

Specifically, PLS-DA model was built using an X matrix containing the spectral data (n rows according to the number of samples and m columns considering the reflectance for each wavelength) and a dependent variable (Y matrix) able to encode the class membership to which the spectra belonged to (1 = VBPR-based and 2 = BS). For model computation, the original spectrum was decomposed into latent variables (LVs) or PLS components that described the variations among the data, showing the utmost covariance among the X and Y variables. The PLS-DA models were cross validated (CV) using Venetian blinds consisting of 10 splits (folds) and a maximum of 20 LVs. The basis of k (10)-fold is that the dataset is split up into an equal-sized subset. Then, the trained model is tested with the remaining sets, operation that is repeated until the established k (10, in this case) folds have undergone the same process. This means that any samples are neither extracted nor omitted from the further model.

Shifting to the second classification approach, RBF-SVM was carried out to perform pattern recognition between two-point classes under the principle of minimizing the structural risk. For that purpose, a decision hyperplane is determined by certain points of the training set, named as support vectors (SV) (Yue et al., 2003). In this case, the machine learning method was trained with a sequential minimal optimization (SMO) (Platt, 1998) to avoid complex analytical numerical solutions ($\gamma = 1$; cost = [0,1; 1,0]; function = gaussian; tolerance = 0.001). As the solver algorithm was applied, each interaction did not require any optimization by itself since it was a simple two-variable classification (Fan et al., 2005).

Apart from the specific parameters of the analyses, the models from both linear and non-linear algorithms were evaluated using both the percentage of Correctly Classified (%CC) samples, also known as accuracy, (Eq. (8)) of predicted fed-class based on a confusion matrix for the train and test sets, and the sensitivity (Eq. (9)) and specificity (Eq. (10)) values based on the True Positives (TP), True Negatives (TN), False Positives (FP), and False Negatives (FN). The closer to 100% the accuracy value and the closer to 1 the sensitivity and specificity values, the more accurate the model performance.

$$\%CC = \frac{TP + TN}{TP + TN + FN + FP} \text{ x } 100 \quad \text{Eq 8}$$

$$\text{Senstivity} = \frac{TP}{TP + FN} \quad \text{Eq 9}$$

$$\text{Specificity} = \frac{TN}{TN + FP} \quad \text{Eq 10}$$

The entire workflow of the study is detailed in Fig. 1.

3. Results and discussion

3.1. Meat quality

Table 1 gathers the descriptive statistics obtained from the physicochemical analysis. Of all the quality parameters, only the total collagen showed statistical differences due to feeding effect (p-value<0.05). Cattle raised in Mediterranean countries, where animals in

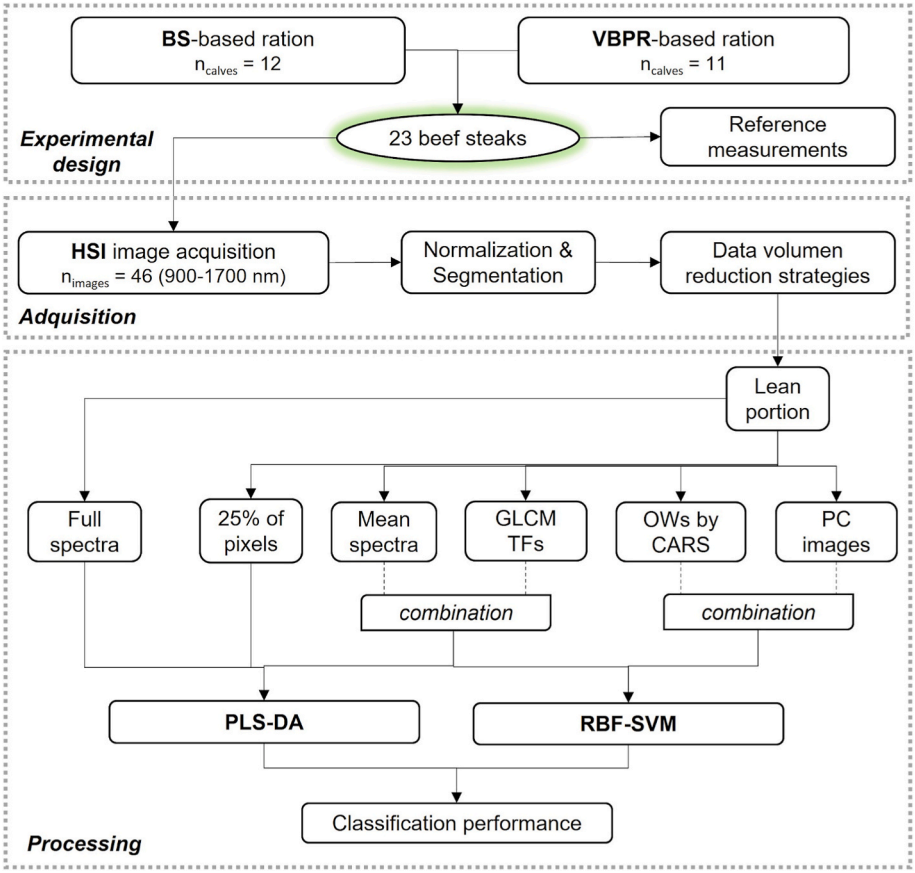

Fig. 1. Workflow of the study carried out to authenticate on meat the diet supplied to fattening calves. BS: conventional feed; VBPR: vegetable by-products based; n: sample number; HSI: hyperspectral imaging; GLCM: gray-level-co-occurrence matrix; OWs: optimal wavelengths: PC: principal component; PLS-DA: partial least square-discriminant analysis; RBF-SVM: radial basis function-support vector machines.

Table 1
Comparison of the physicochemical composition (mean ± standard deviation) of meat samples from barley and straw and vegetable by-products-fed cattle by ANOVA.

	BS	VBPR	p-value
Chemical composition			
IMF, %	3.14 ± 1.25	2.91 ± 1.13	0.650
Protein, %	22.14 ± 0.56	21.88 ± 0.64	0.301
Quality traits			
WBSF (N cm^{-2})	41.12 ± 7.03	38.61 ± 9.91	0.489
Soluble collagen (mg g^{-1} sample)	0.47 ± 0.18	0.47 ± 0.16	0.997
Total collagen (mg g^{-1} sample)	4.28^{b} ± 0.96	5.34^{a}±1	0.017
Meat color traits			
L*	37.7 ± 1.83	37.21 ± 1.54	0.507
a*	20.07 ± 1.23	19.62 ± 1.4	0.431
b*	4.73 ± 0.96	4.32 ± 0.95	0.316
C*	20.67 ± 1.22	20.13 ± 1.46	0.365
h*	13.16 ± 2.68	18.71 ± 21.6	0.407

VBPR: vegetable by-products based; BS: conventional feed; N: newtons; L*: lightness; a*: redness; b*: yellowness, C*: chroma; h*: hue. p-value <0.05: significant diet effect.

their fattening period are supplied concentrate and straw, generally present lower contents of total collagen because it is diluted by the higher protein rate (Archile-Contreras et al., 2010). This statement is in accordance with the results obtained in this study since the BS-based ration showed lower contents of total collagen than the VBPR-based ration. Notwithstanding, the total collagen content obtained in both scenarios was higher than the 3.18 ± 0.09 mg g^{-1} reported by other authors (Christensen et al., 2011).

Closely related to collagen is tenderness. WBSF showed lower mean values for the VBPR-finished beef compared to those supplied a conventional ration (38.41 vs. 41.12N cm^{-2}). Regarding those values and according to the American Meat Science Association (2016) the meat steaks were classified as "tender" (39 < WBSF >32N cm^{-2}) for VBPR and "intermediate" for BS as the 39N limit was exceeded but was not higher than 46N. These results were supported by previous studies, for instance, Panea et al. (2018) reported 38N values in average (n = 55) for purebred Pirenaica meat.

Concerning intramuscular fat (IMF), in agreement with Wood et al. (2008), the meat coming from concentrate-fed calves showed a higher content when compared with high forage diets-fed beef. Nevertheless, in our study, no significant differences were found.

Another meat quality parameter that varies with diet is color. Aligned with the results from the present study, Albertí et al. (2014) reported a L* value of 42.2 for Pirenaica calves fed during 75 days with an isocaloric and isoproteic concentrate. Among the BS and VBPR meat there were no differences for color, key aspect since it is the most important parameter considered by consumers at the time of purchase (Salim et al., 2022). According to the obtained results, no discrimination at an early look could be encountered among both products.

3.2. Spectra interpretation

Fig. 2a represents the mean spectrum of the two groups of meat from the BS vs. VBPR feeding trial in the 1038–1700 nm NIR spectral range. In it, the common groups of the main constituents of meat are manifested by the intensity of the absorption bands. In both types of fresh meat reflectance curves of similar shape along the spectral range measured were found. The main difference resided on the magnitude of the reflectance, starting from 1350 nm (Fig. 2b), increasing from 1400 nm and above, where the BS group registered narrowly higher values than those acquired by the VBPR one. As water is the main component of beef meat, this gap may be due to the water absorption and moisture content of the steaks, which is expressed by the O–H first and second overtones (Williams & Norris, 2001). A slightly higher moisture content of 0.25% was obtained in the VBPR meat compared to the BS (data not shown). Therefore, the VBPR meat slightly stood out for absorbing a larger amount of near infrared radiation in the 900–1700 nm spectral range when comparing it with the BS meat, reflecting in both products a score of no more than 0.04. Therefore, although in a very subtle manner, we hypothesized that the amount of water in the beef muscle had an influence in the reflectance spectra.

Also, it is around 1400–1500 nm were the first overtone N–H stretching is manifested, which is correlated to protein. Certainly, featured absorption peaks around 1250 nm are associated with the appearance of fat due to the presence of –CH═CH– vibrations on the second overtone, i.e., fatty acids which also vary according to the nutrition provided to the animals (Williams & Norris, 2001). In the present study, even if the differences were small, C18:2, C18:3, C20:4, C20:5 and C22:6 showed higher content in VBPR than in BS samples (data not shown).

3.3. Data volume reduction strategies

3.3.1. Selection of effective wavelengths

To extract the optimal wavelengths from the full spectral range (1038–1700 nm) and to simplify the model performance associated to the diet supplied to fattening calves, the CARS method was computed. The distribution of the 150 useful variables that were identified for

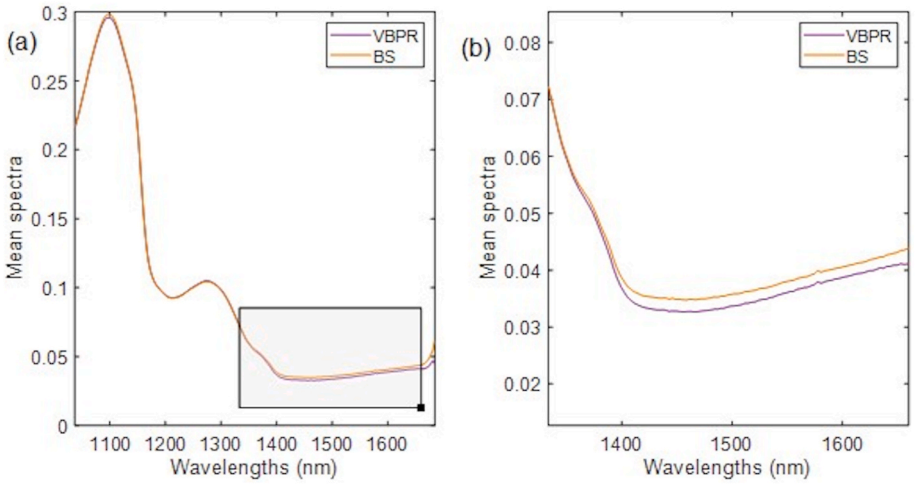

Fig. 2. Mean reflectance spectra of the meat obtained from calves with two different finishing diets: (a) full spectrum captured by the NIR-HSI camera from 1038 to 1700 nm; (b) zoom in the 1300–1700 nm range.

further beef meat classification can be seen in Fig. 3b together with the RMSECV registered for each CARS iteration made (Fig. 3a). As it can be seen, the distribution of the 150 selected wavelengths is quite homogenously spread along the spectrum.

3.3.2. PC score images

By means of the Principal Component Analysis the optimal characteristic images were computed. The first three PC images were extracted (Fig. 4), explaining 81.72%, 8.22% and 4.82% of the total variance for PC1, PC2 and PC3, respectively. It can be said that PC1 was the best representation of the original sample itself. Other authors as Wang et al. (2020) obtained similar results for lamb meat in terms of cumulative spectral variance (85.88%).

3.3.3. Texture feature analysis of hyperspectral images

Fig. 5 stands for the average texture features profiles of the hyperspectral images belonging to the steaks in the 1038–1700 nm range.

Pearson's correlation coefficient was calculated among the average of the five texture values and both sample categories. Only entropy complied with the requirements set up in the study (p-value$<$0.05) whereas correlation only registered a tendency ($COR_{p\text{-value}} = 0.11$). The remaining parameters were not correlated with the feeding effect ($CON_{p\text{-value}} = 0.41$; $ENE_{p\text{-value}} = 0.37$; $HOM_{p\text{-value}} = 0.41$). Therefore, to authenticate the samples according to the feeding provided to the animals, only the entropy values for each wavelength were extracted to be further combined with the mean spectrum of each steak.

3.4. Data classification: VBPR-fed beef authentication

3.4.1. Linear and non-linear discrimination approaches

Linear (PLS-DA) and non-linear (RBF-SVM) discrimination approaches were applied to the intact LDL muscle for BS and VBPR-fed calves and the obtained results are shown in Table 2. The best results are exposed in terms of Correctly Classified samples of each group in train and test sets (in bold). Classification models were run based on either full spectrum, OWs selection, mean spectra (MS), or selection of the 25% pixels as for the entire steak.

For PLS-DA models, the overall accuracy percentage of CC ranged from 65.72 to 74.02% for train and from 58.33 to 65.69% for test, for all the pre-processing applied, also including the non-application of any of them (Raw data). As a case in point, the % of correctly identified samples for train were higher for the barley and straw samples, with up to 88.89% only when the mean spectra were included whereas when the variables selected by the CARS method were involved, the %CC was slightly reduced to 88.70%. Similar studies tried to authenticate meat based on the finishing feed provided. Barragán et al. (2021) discriminated, using a Vis-NIR instrument combined with a PLS-DA model, among barley, blend, and corn-fed cattle, obtaining an accuracy of 57, 46 and 48%, respectively, in CV using intact *Longissimus thoracis* muscle.

However, a common trend for both feeding groups was seen when the samples were externally validated, as the %CC decreased regardless the number of wavelengths included. Despite this, the %CC rates obtained in the present study were better for the samples coming from animals finished with barley and straw, proving a linearity among spectra and BS. This difference can be explained by the fact that BS-finished calves had a higher fat and protein content. Patel et al. (2021) affirmed how NIRS prediction basis lies on functional groups of different organic molecules, this is, the expected predictability of dry matter, lipids and proteins are likely to be higher. Indeed, it could be inferred how in the steaks of a BS-based ration, the molecules are more clustered than in those fed VBPR, which is probably due to a more homogeneous meat.

Secondly, when analyzing the results of the RBF-SVM approach (Table 2), the overall accuracy varied from 49.12 to 68.96% for train and from 41.87 to 68.60% for test. In detail, the percentage of CC for train dataset for the VBPR-finished animals ranged from 46.73 up to 87.50%, according to the SRS method run and the further pre-processing applied. Contrary, BS-finished meat presented less variability for test, where the rate of CC, either pixels or spectrum-based, ranged from 57.14 up to 68.06%. The best results were reached for those data obtained through the application of CARS that were no subjected to a posterior treatment (81.97 and 64.19% for VBPR and BS in the train dataset, respectively).

Overall, the RBF-SVM achieved better classifications for the VBPR group than the PLS-DA, while for the BS meat the opposite situation was true for machine learning methods. In terms of general accuracy for train and test, PLS-DA registered higher ratios of authenticated meat cuts than RBF-SVM. In this line, Sanz et al. (2016) performed a discrimination amongst different lamb muscles using HSI. They obtained a success rate of 83.33% for the concrete case of the *Semimembranosus* muscle using a SVM algorithm. As can be noted, the present study goes a step further in the state-of-the-art since a single muscle was used for both treatment groups. Unlike prediction models in the NIR spectral range, which do not consider spatial information as HSI does, in the present study, spectral data collection was carried out while maintaining muscle integrity, which had a positive impact on the grading performance (Robert et al., 2023).

However, BS meat did not show as wide variability for %CC as the VBPR feed, which confirms, from a spectral point of view, that meat quality could be modified through feeding. This fact is mainly linked to how calves metabolize ration intake, also related to their genetics and biological processes (Jelan & Sumarmono, 2019). Geay and Robelin (1979) affirmed how a diet based on a high energy content enables each breed or genotype to express their feed intake capacity, which is linked

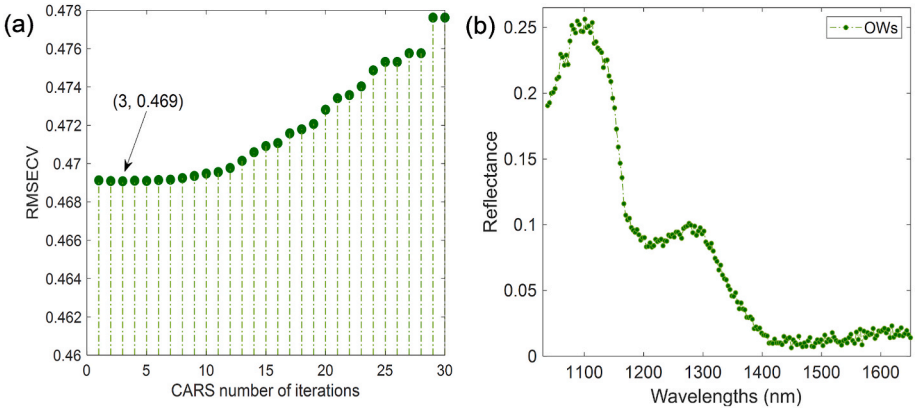

Fig. 3. Selection of optimal wavelengths through CARS algorithm: (a) RMSECV registered for the iterations carried out to finally select the minimum error registered; and (b) distribution of the 150 OWs.

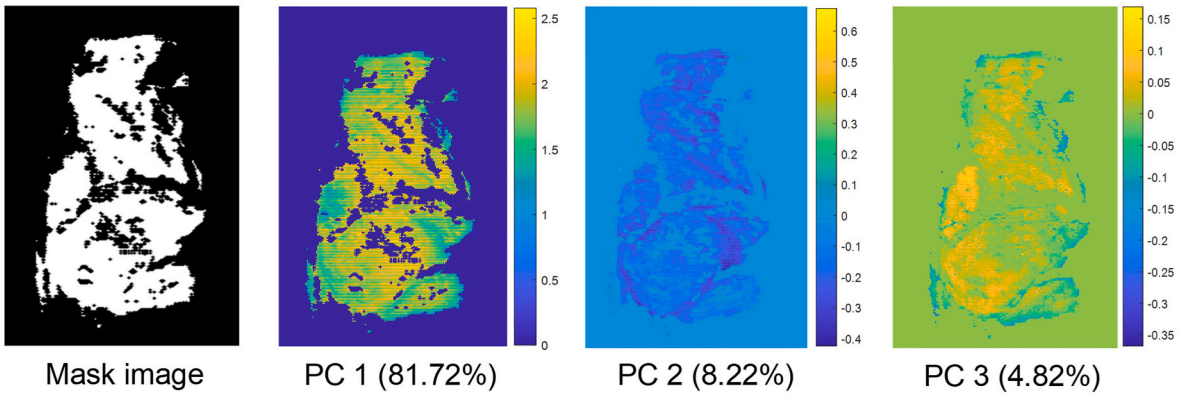

Fig. 4. Registered scores of the first 3 PCs.

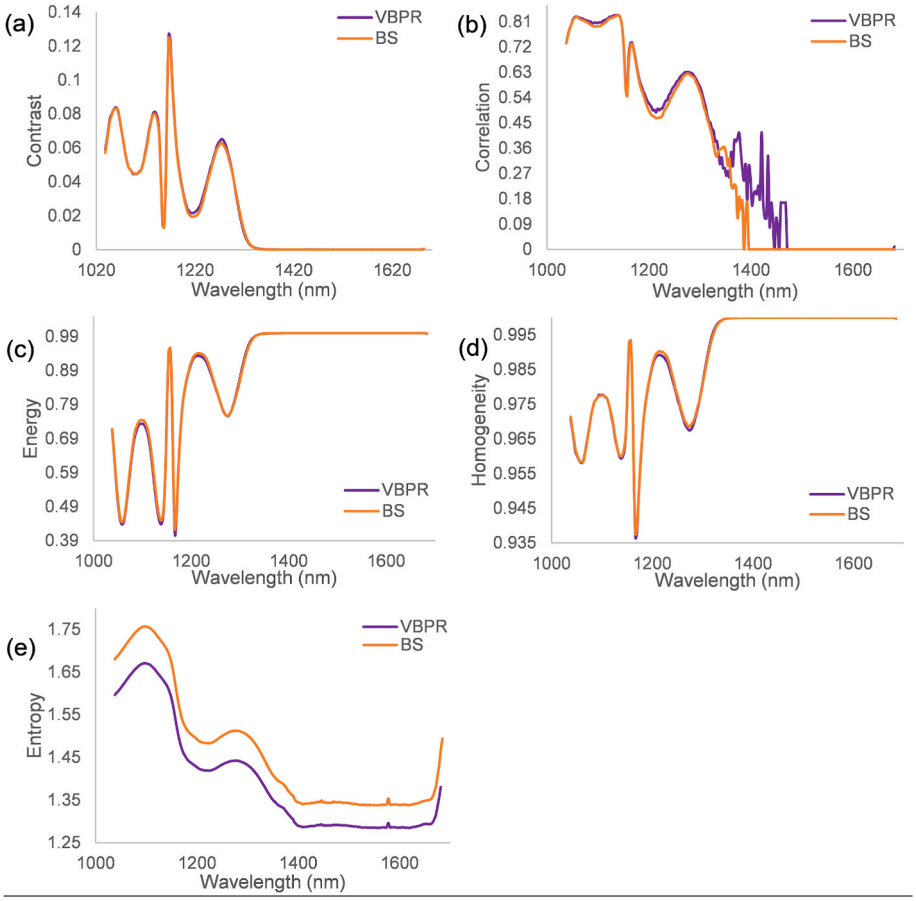

Fig. 5. Texture features profile ((a) Contrast, (b) Correlation, (c) Energy, (d) Homogeneity and (e) Entropy) of the hyperspectral images obtained from the steaks according to the feedstuff supplied to the fattening calves (BS: barley and straw feeding; VBPR: vegetable by-products-based feeding).

to the feed efficiency on muscular growth, protein retention capacity, variations of body weight gain, and the distribution of energy intake among maintenance and production. In the present study, the calves came from a Pirenaica purebred which approach has changed in the course of the years and is currently focused mainly on beef production (Álvarez-Rodríguez & Sanz, 2009). Furthermore, all the parameters considered in the selection programs (i.e., morphology, production rates, intake capacity, etc.) are related to the conventional feed ration that has traditionally been provided. Hence, the calves' ability to adapt to novel feed can produce variations in the subsequent meat (Ornaghi et al., 2020).

Table 3 shows the sensitivity and specificity values obtained for the best results (in terms of %CC) of the PLS-DA and RBF-SVM models. Regarding the former, the best performing results were recorded for the full spectrum model (in train, 54.65 and 83.66%, Table 2), followed in second position by the one obtained from CARS variable selection (in train, 53.50 and 83.88%). In both SRS scenarios, the pixels of BS meat graded better compared to VBPR. These data show that the %CC of VBPR is close to the proportion of barley included in the VBPR ration (53.08% of the total), which, with the addition of straw content (4.07%), were close to 60% of the total.

With the second machine learning algorithm (RBF-SVM), higher classification values were achieved by the Raw data after CARS variable selection, in comparison to MS and the selection of 25% of pixels within

Table 2
Partial least square and radial basis function-support vector machine discrimination analysis of meat samples from barley and straw and vegetable by-products-fed cattle.

						CC (%) for Train			CC (%) for Test		
Model	MP	LV	n Train	n Test	SRS	BS	VBPR	Accuracy (%)	BS	VBPR	Accuracy (%)
PLS-DA											
	Raw data	6	837,840	224,460	/	83.30	52.25	67.78	80.29	45.17	62.73
	SM + MC	5	827,212	225,912	/	83.66	54.65	**69.15**	79.27	50.15	**64.82**
	1st der + MC	9	791,389	217,081	/	82.75	58.71	70.73	79.04	46.74	62.89
	SM + MSC + MC	6	785,096	221,476	/	81.36	60.50	70.93	78.03	45.00	61.51
	SM + SNV + MC	5	837,806	233,680	CARS	82.83	52.55	67.69	79.99	48.19	64.09
	Raw data	7	837,722	233,655	CARS	83.35	52.37	67.86	81.08	47.12	64.10
	SM + MC	7	835,099	233,668	CARS	83.88	53.50	**68.69**	80.57	50.26	**65.42**
	1st der + SNV + MC	3	835,755	232,677	CARS	88.70	43.60	66.15	87.81	35.47	61.64
	SM + MSC + MC	5	837,244	233,563	CARS	82.91	52.49	67.70	80.22	48.17	64.20
	1st der + MC	1	35	9	MS	88.89	58.82	**73.86**	83.33	33.33	**58.33**
	1st der + SNV + MC	3	35	9	MS	83.33	64.71	74.02	83.33	33.33	58.33
	SM + MC	5	208,419	58,430	25%px	83.34	54.45	**68.89**	79.02	52.37	**65.69**
	1st der + MC	5	200,803	58,430	25%px	81.11	50.35	65.72	76.90	52.62	64.76
	1st der + MSC + MC	8	189,412	53,156	25%px	85.12	61.50	73.31	82.44	46.04	64.24
RBF-SVM											
	Raw data	/	837,856	233,713	CARS	64.19	81.97	**68.96**	68.06	70.69	**68.60**
	SM + SNV + MC	/	837,856	233,713	CARS	51.74	48.12	50.30	61.42	41.95	53.46
	Raw data	/	36	10	MS	63.64	71.43	66.67	57.14	33.33	50.00
	SM + MSC + MC	/	36	10	MS	60.71	87.50	**66.67**	62.50	50.00	**60.00**
	1st der + SNV + MC	/	209,464	58,430	25%px	51.64	46.73	**51.17**	59.85	38.44	**57.43**
	SM + MC	/	209,464	58,430	25%px	60.71	48.54	49.12	60.71	40.02	41.87

MP: mathematical pre-processing; LV: latent variables selected; n: number of pixels/samples used; SRS: spectral reduction strategy; BS: barley and straw feeding; VBPR: vegetable by-products-based feeding; CC: correctly classified; MC: mean center; SM: smoothing; MSC: mean scatter correction; SNV: standard normal variate; 1st der: first derivative; MS: mean spectra; 25%px: 25% of the pixels from the lean portion.

Table 3
Best sensitivity and specificity values obtained by the PLS-DA and RBF-SVM Test dataset according to the different spectral reduction strategies performed.

SRS	MP	LV	Sensitivity		Specificity	
			BS	VBPR	BS	VBPR
PLS-DA						
/	SM + MC	5	0.805	0.413	0.413	0.805
CARS	SM + MC	7	0.820	0.376	0.376	0.820
MS	1st der + MC	1	0.833	0.333	0.333	0.833
25%px	SM + MC	5	0.808	0.378	0.378	0.808
RBF-SVM						
CARS	Raw data	/	0.681	0.707	0.707	0.681
MS	SM + MSC + MC	/	0.625	0.500	0.500	0.625
25%px	1st der + SNV + MC	/	0.384	0.599	0.599	0.384

SRS: spectral reduction strategy; MP: mathematical pre-processing; LV: latent variables selected; VBPR: vegetable by-products based; BS: barley and straw feeding; MC: mean center; SM: smoothing; 1st der: first derivative; CARS: competitive adaptive reweighted sampling; MS: mean spectra; 25%px: 25% of the pixels from the lean portion.

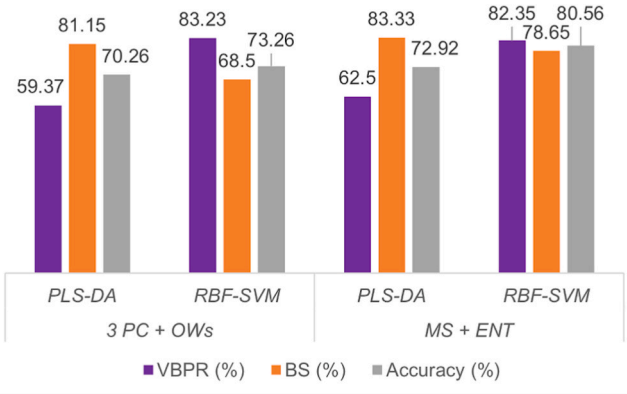

Fig. 6. Comparison of the Train performance of the PLS-DA and RBF-SVM classification models based on spectral and textural features combination of HSI. BS: barley and straw feeding; VBPR: vegetable by-products-based feeding.

the steak.

3.4.2. Combination of spectral and textural data of HSI

After block variance scaling to overcome the dissimilarities among data matrixes, PLS-DA and RBF-SVM classification models were built based on data combination with no pre-processing. First, the 3 PC images, explaining the 94.76% of the total variance together with the 150 variables selected by the CARS method, were merged. Then, to overcome the large data volume generated, the mean spectrum of each sample was combined with entropy as it highlighted as the unique effective texture feature. Once the matrixes were merged, the multivariate analysis methods were set up, as it is summarized in Fig. 6. Compared to the results obtained from the original models, both combination methodologies showed promising and competent results.

The outcomes from the present study noted a non-linear relationship among the VBPR group and the spectrum while the linearity among the PLS-DA method and BS was enhanced. All the feature joint models (3 PC + OWs; MS + ENT) were able to satisfactorily classify the LDL steaks into the two categories (>70% of overall accuracy). Moreover, the overall accuracy obtained by the combined RBF-SVM mean spectra and entropy model surpassed the 80% of CC, which also resulted in 82.35% authenticated VBPR. ENT therefore played a key role in classifying the meat steaks according to diets, which in turn, combined with the mean spectrum in the NIR range, enhanced and maximized the performance of the models. Since total collagen was the unique meat quality parameter that showed significance from the physicochemical analysis, it could be affirmed how the distribution of collagen influenced the ENT of the HSI images. Nevertheless, Xiong et al. (2015) explained how, meat fatty acids could directly or indirectly affect the texture of the muscle images due to fiber characteristics. So, ENT, which is associated to the randomness of the HSI images, might be influenced by the quantity of fatty acids present in the meat. These compounds may vary mainly with the diet supplied; therefore, the textural feature ENT may reveal the feeding effect. Wang et al. (2020) explained how, for lamb, the models that combined spectral and TF data acquired higher scores as the

internal chemical composition of the meat influenced more than the surface physical information.

Furthermore, it should be emphasized that the VBPR-based ration enables the closing of the loop in the food chain through circular economy techniques, enhancing the sustainability of the livestock activity. A key aspect of this type of meat livestock system is that it is rooted in the environment in which the activity takes place, thus contributing to the local economy. As López-Maestresalas et al. (2019) affirmed, this kind of authentication studies are of great importance when the products come from local breeds reared under sustainable conditions that constitute PGIs ("Ternera de Navarra", in this case). HSI technology could be applied to discriminate among meat from calves finished with different diets guaranteeing the sustainability of the production and highlighting the added value of the livestock sector activity. It therefore has a beneficial effect on the digitization of quality processes and on the confidence placed in animal products.

4. Conclusions

The meat from calves finished on a ration incorporating local vegetable by-products showed a quality composition similar to that of animals finished with a traditional feedstuff based on barley and straw. Therefore, given the innovation of the product, it is necessary to develop a rapid, reliable, *on-line,* and *at-line* control technology capable of authenticating the meat and highlighting such information at the time of purchase, which in turn has a positive impact on the beef sector. For that purpose, two machine learning discrimination methods were able to differentiate among the beef steaks. PLS-DA registered higher correctly classified pixels or spectrum rates for train (65.72–74.02%) than RBF-SVM models (49.12–68.96%). However, the best results were obtained thanks to the combination of spectral and textural data of HSI. The merger among spectral (i.e., Mean spectra) and texture features (i.e., Entropy) of hyperspectral imaging was able to authenticate the diet supplied to fattening calves with and overall accuracy >80%. For future research, it would be interesting to test these findings in other animal species also VBPR fed and their products (milk, cheese, eggs) with the aim of diversifying the products offered to the market, while boosting the sustainability of the livestock farming.

CRediT authorship contribution statement

Sara León-Ecay: Conceptualization, Data curation, Formal analysis, Investigation, Validation, Visualization, Writing – original draft. **Kizkitza Insausti:** Conceptualization, Funding acquisition, Investigation, Methodology, Project administration, Supervision, Writing – review & editing, Resources. **Silvia Arazuri:** Conceptualization, Data curation, Formal analysis, Software, Supervision, Writing – review & editing, Resources. **Irantzu Goenaga:** Conceptualization, Funding acquisition, Investigation, Project administration, Supervision, Writing – review & editing. **Ainara López-Maestresalas:** Conceptualization, Data curation, Formal analysis, Investigation, Methodology, Resources, Software, Supervision, Validation, Writing – review & editing.

Declaration of competing interest

The authors declare that they have no known competing financial interest or personal relationships that could have appeared to influence the work reported in this paper.

Data availability

Data will be made available on request.

Acknowledgments

This research was funded by Universidad Pública de Navarra through a PhD scholarship (UPNA-2022 (Res.2178/2022)), by the Government of Navarra in the framework of an Industrial PhD 2020 scholarship (0011-1408-2020-000009), and by the Government of Navarra and the European Regional Development Fund (ERDF) via project BEEF+ "*Carne saludable a través de la economía circular*" 0011-1365-2020-000288. Open access funding provided by Universidad Pública de Navarra.

References

Acharya, D., Rani, A., Agarwal, S., & Singh, V. (2016). Application of adaptive Savitzky–Golay filter for EEG signal processing. *Perspectives in Science, 8*, 677–679. https://doi.org/10.1016/j.pisc.2016.06.056

Albertí, P., Beriain, M. J., Ripoll, G., Sarriés, V., Panea, B., Mendizabal, J. A., Purroy, A., Olleta, J. L., & Sañudo, C. (2014). Effect of including linseed in a concentrate fed to young bulls on intramuscular fatty acids and beef color. *Meat Science, 96*(3), 1258–1265. https://doi.org/10.1016/j.meatsci.2013.11.009

Álvarez-Rodríguez, J., & Sanz, A. (2009). Physiological and behavioural responses of cows from two beef breeds submitted to different suckling strategies. *Applied Animal Behaviour Science, 120*(1–2), 39–48. https://doi.org/10.1016/j.applanim.2009.05.004

American Meat Science Association. (2016). *Research guidelines for cookery, sensory evaluation, and instrumental tenderness measurements of meat*. American Meat Science Association Educational Foundation. http://www.meatscience.org.

Aouat, S., Ait-hammi, I., & Hamouchene, I. (2021). A new approach for texture segmentation based on the Gray Level Co-occurrence Matrix. *Multimedia Tools and Applications, 80*(16), 24027–24052. https://doi.org/10.1007/s11042-021-10634-4

Archile-Contreras, A. C., Mandell, I. B., & Purslow, P. P. (2010). Disparity of dietary effects on collagen characteristics and toughness between two beef muscles. *Meat Science, 86*(2), 491–497. https://doi.org/10.1016/j.meatsci.2010.05.041

Attrey, D. P. (2017). Role of public health food safety laboratories in detection of adulterants/contaminants. In *Food safety in the 21st century* (pp. 161–175). Elsevier. https://doi.org/10.1016/B978-0-12-801773-9.00012-1.

Barragán, W., Aalhus, J. L., Penner, G., Dugan, M. E. R., Juárez, M., López-Campos, Ó., Vahmani, P., Segura, J., Angulo, J., & Prieto, N. (2021). Authentication of barley-finished beef using visible and near infrared spectroscopy (Vis-NIRS) and different discrimination approaches. *Meat Science, 172*, Article 108342. https://doi.org/10.1016/j.meatsci.2020.108342

Basantia, N. C., Nollet, L. M. L., & Kamruzzaman, M. (Eds.). (2019). *Hyperspectral imaging analysis and applications for food quality*. CRC Press, Taylor & Francis Group.

Bharat Helkar, P., & Sahoo, A. (2016). Review: Food industry by-products used as a functional food ingredients. *International Journal of Waste Resources, 6*(3). https://doi.org/10.4172/2252-5211.1000248

Bian, X. (2022). Spectral preprocessing methods. In X. Chu, Y. Huang, Y.-H. Yun, & X. Bian (Eds.), *Chemometric methods in analytical spectroscopy technology* (pp. 111–168). Springer Nature Singapore. https://doi.org/10.1007/978-981-19-1625-0_4.

Biancolillo, A., Marini, F., Ruckebusch, C., & Vitale, R. (2020). Chemometric strategies for spectroscopy-based food authentication. *Applied Sciences, 10*(18), 6544. https://doi.org/10.3390/app10186544

Bonnet, M., & Kopp, J. (1992). Préparation des échantillons pour le dosage et la caractérisation qualitative du collagène musculaire. *Viandes et Produits Carnes, 13*, 87–91.

Christensen, M., Ertbjerg, P., Failla, S., Sañudo, C., Richardson, R. I., Nute, G. R., Olleta, J. L., Panea, B., Albertí, P., Juárez, M., Hocquette, J.-F., & Williams, J. L. (2011). Relationship between collagen characteristics, lipid content and raw and cooked texture of meat from young bulls of fifteen European breeds. *Meat Science, 87*(1), 61–65. https://doi.org/10.1016/j.meatsci.2010.09.003

de Agricultura, Ministerio, & Alimentación, Pesca y (2000). *Real Decreto 348/2000, de 10 de marzo, por el que se incorpora al ordenamiento jurídico la Directiva 98/58/CE, relativa a la protección de los animales en las explotaciones ganaderas*.

Despoudi, S., Bucatariu, C., Otles, S., Kartal, C., Otles, S., Despoudi, S., Bucatariu, C., & Kartal, C. (2021). Food waste management, valorization, and sustainability in the food industry. In *Food waste recovery* (pp. 3–19). Elsevier. https://doi.org/10.1016/B978-0-12-820563-1.00008-1.

The Dublin Declaration of Scientists on the societal role of livestock. *Animal Frontiers, 13*(2), (2023), 10. https://doi.org/10.1093/af/vfad013, 10.

EEC. (1993). *Council Directive 93/119/EC of 22 December 1993 on the protection of animals at the time of slaughter or killing*.

EEC. (2004). Commission Regulation (EC) No 1483/2004 of 20 August 2004 supplementing the Annex to Regulation (EC) No 2400/96 on the entry of certain names in the Register of protected designations of origin and protected geographical indications ('Carne de la Sierra d. *Official Journal of the European Union, 273*, 3–4.

EEC. (2010). *Directive 2010/63/EU of the European Parliament and of the Council of 22 September 2010 on the protection of animals used for scientific purposes*.

ElMasry, G., Sun, D.-W., & Allen, P. (2011). Non-destructive determination of water-holding capacity in fresh beef by using NIR hyperspectral imaging. *Food Research International, 44*(9), 2624–2633. https://doi.org/10.1016/j.foodres.2011.05.001

Espinosa-Alonso, L. G., Valdez-Morales, M., Aparicio-Fernandez, X., Medina-Godoy, S., & Guevara-Lara, F. (2020). Vegetable By-products. In R. Campos-Vega, B. D. Oomah, & H. A. Vergara-Castañeda (Eds.), *Food wastes and by-products* (1st ed., pp. 223–266). Wiley. https://doi.org/10.1002/9781119534167.ch8.

Fan, R.-E., Chen, P.-H., & Lin, C.-J. (2005). Working set selection using second order information for training support vector machines. *Journal of Machine Learning Research, 6*, 1889–1918.

Fassio, F., Borda, I. E. P., Talpo, E., Savina, A., Rovera, F., Pieretto, O., & Zarri, D. (2022). Assessing circular economy opportunities at the food supply chain level: The case of five piedmont product chains. *Sustainability, 14*(17), Article 10778. https://doi.org/10.3390/su141710778

Feng, Y. Z., & Sun, D. W. (2012). Application of hyperspectral imaging in food safety inspection and control: A review. *Critical Reviews in Food Science and Nutrition, 52*(11), 1039–1058. https://doi.org/10.1080/10408398.2011.651542

Fisher, R. A. (1992). Statistical methods for research workers. In S. Kotz, & N. L. Johnson (Eds.), *Breakthroughs in statistics* (pp. 66–70). Springer New York. https://doi.org/10.1007/978-1-4612-4380-9_6.

Gade, A. A., & Vyavahare, A. J. (2018). Feature extraction using GLCM for dietary assessment application. *International Journal of Multimedia and Image Processing, 8*(2), 409–413. https://doi.org/10.20533/ijmip.2042.4647.2018.0050

Geay, Y., & Robelin, J. (1979). Variation of meat production capacity in cattle due to genotype and level of feeding: Genotype-nutrition interaction. *Livestock Production Science, 6*(3), 263–276. https://doi.org/10.1016/0301-6226(79)90044-7

Godfray, H. C. J., Aveyard, P., Garnett, T., Hall, J. W., Key, T. J., Lorimer, J., Pierrehumbert, R. T., Scarborough, P., Springmann, M., & Jebb, S. A. (2018). *Meat consumption, health, and the environment.* New York, N.Y.: Science. https://doi.org/10.1126/science.aam5324, 6399.

Goenaga, I., García-Rodríguez, A., Goiri, I., León-Ecay, S., De Las Heras, J., Aldai, N., & Insausti, K. (2023). Vegetable by-products as alternative and sustainable raw materials for ruminant feeding: Nutritive evaluation and their inclusion in a novel ration for calf fattening. *Animals, 13*(8), 1391. https://doi.org/10.3390/ani13081391

Haralick, R. M., Shanmugam, K., & Dinstein, I. (1973). Textural features for image classification. *IEEE Transactions on Systems, Man, and Cybernetics, SMC-, 3*(6), 610–621. https://doi.org/10.1109/TSMC.1973.4309314

Hawlick, R. M. (1979). Statistical and structural approaches to texture. *Proceedings of the IEEE, 67*(5), 786–804.

ISO 1443:1973. (1973). Meat and meat products—determination of total fat content. In *International Organization of Standarization (Meat, poultry, fish, eggs and their products)*.

ISO 937:1978. (1978). Meat and meat products—determination of nitrogen content (Reference method). *International Organization of Standarization (Meat, poultry, fish, eggs and their products)*.

Jelan, Z. A., & Sumarmono, J. (2019). Nutritional manipulations and its effects on yield and quality of beef. *IOP Conference Series: Earth and Environmental Science, 372*(1), Article 012066. https://doi.org/10.1088/1755-1315/372/1/012066

Jia, W., van Ruth, S., Scollan, N., & Koidis, A. (2022). Hyperspectral Imaging (HSI) for meat quality evaluation across the supply chain: Current and future trends. *Current Research in Food Science, 5*, 1017–1027. https://doi.org/10.1016/j.crfs.2022.05.016

Katemala, S., Molee, A., Thumanu, K., & Yongsawatdigul, J. (2021). Meat quality and Raman spectroscopic characterization of Korat hybrid chicken obtained from various rearing periods. *Poultry Science, 100*(2), 1248–1261. https://doi.org/10.1016/j.psj.2020.10.027

Kucha, C. T., Liu, L., Ngadi, M., & Gariépy, C. (2022). Improving intramuscular fat assessment in pork by synergy between spectral and spatial features in hyperspectral image. *Food Analytical Methods, 15*(1), 212–226. https://doi.org/10.1007/s12161-021-02113-1

Li, X., Cai, M., Li, M., Wei, X., Liu, Z., Wang, J., Jia, K., & Han, Y. (2023). Combining Vis-NIR and NIR hyperspectral imaging techniques with a data fusion strategy for the rapid qualitative evaluation of multiple qualities in chicken. *Food Control, 145*, Article 109416. https://doi.org/10.1016/j.foodcont.2022.109416

Li, H., Liang, Y., Xu, Q., & Cao, D. (2009). Key wavelengths screening using competitive adaptive reweighted sampling method for multivariate calibration. *Analytica Chimica Acta, 648*(1), 77–84. https://doi.org/10.1016/j.aca.2009.06.046

Liu, D., Pu, H., Sun, D.-W., Wang, L., & Zeng, X.-A. (2014). Combination of spectra and texture data of hyperspectral imaging for prediction of pH in salted meat. *Food Chemistry, 160*, 330–337. https://doi.org/10.1016/j.foodchem.2014.03.096

López-Maestresalas, A., Insausti, K., Jarén, C., Pérez-Roncal, C., Urrutia, O., Beriain, M. J., & Arazuri, S. (2019). Detection of minced lamb and beef fraud using NIR spectroscopy. *Food Control, 98*, 465–473. https://doi.org/10.1016/j.foodcont.2018.12.003

Ma, J., Sun, D.-W., Pu, H., Cheng, J.-H., & Wei, Q. (2019). Advanced techniques for hyperspectral imaging in the food industry: Principles and recent applications. *Annual Review of Food Science and Technology, 10*(1), 197–220. https://doi.org/10.1146/annurev-food-032818-121155

Malavi, D., Nikkhah, A., Raes, K., & Van Haute, S. (2023). Hyperspectral imaging and chemometrics for authentication of extra virgin olive oil: A comparative approach with FTIR, UV-VIS, Raman, and GC-MS. *Foods, 12*(3), 429. https://doi.org/10.3390/foods12030429

Nardella, S., Conte, A., & Del Nobile, M. A. (2022). State-of-Art on the recycling of by-products from fruits and vegetables of mediterranean countries to prolong food shelf life. *Foods, 11*(5), 665. https://doi.org/10.3390/foods11050665

Novaković, S., & Tomašević, I. (2017). A comparison between warner-bratzler shear force measurement and texture profile analysis of meat and meat products: A review. *IOP Conference Series: Earth and Environmental Science, 85*, Article 012063. https://doi.org/10.1088/1755-1315/85/1/012063

Ornaghi, M. G., Guerrero, A., Vital, A. C. P., de Souza, K. A., Passetti, R. A. C., Mottin, C., de Araújo Castilho, R., Sañudo, C., & do Prado, I. N. (2020). Improvements in the quality of meat from beef cattle fed natural additives. *Meat Science, 163*, Article 108059. https://doi.org/10.1016/j.meatsci.2020.108059

Panea, B., Olleta, J. L., Sañudo, C., Campo, M., del, M., Oliver, M. A., Gispert, M., Serra, X., Renand, G., Oliván, M., del, C., Jabet, S., García, S., López, M., Izquierdo, M., García-Cachán, M. D., Quintanilla, R., & Piedrafita, J. (2018). Effects of breed-production system on collagen, textural, and sensory traits of 10 European beef cattle breeds. *Journal of Texture Studies, 49*(5), 528–535. https://doi.org/10.1111/jtxs.12350

Park, B., Shin, T., Cho, J.-S., Lim, J.-H., & Park, K.-J. (2023). Improving blueberry firmness classification with spectral and textural features of microstructures using hyperspectral microscope imaging and deep learning. *Postharvest Biology and Technology, 195*, Article 112154. https://doi.org/10.1016/j.postharvbio.2022.112154

Patel, N., Toledo-Alvarado, H., & Bittante, G. (2021). Performance of different portable and hand-held near-infrared spectrometers for predicting beef composition and quality characteristics in the abattoir without meat sampling. *Meat Science, 178*, Article 108518. https://doi.org/10.1016/j.meatsci.2021.108518

Platt, J. C. (1998). Fast training of support vector machines using sequential minimal optimization. In *Advances in kernel methods—support vector learning* (pp. 185–208). MIT Press.

Prieto, N., Osika, E., Aalhus, J. L., Lopez-Campos, O., Juarez, M., & Pawluczyk, O. (2018). Application of hyperspectral imaging on meat and meat products. *CABI Reviews*, 1–11. https://doi.org/10.1079/PAVSNNR201813042, 2018.

Rao, M., Bast, A., & de Boer, A. (2021). Valorized food processing by-products in the EU: Finding the balance between safety, nutrition, and sustainability. *Sustainability, 13*(8), 4428. https://doi.org/10.3390/su13084428

Reis, M. M., Beers, R. V., Al-sarayreh, M., Shorten, P., Qi, W., Saeys, W., Klette, R., & Craigie, C. (2018). Chemometrics and hyperspectral imaging applied to assessment of chemical , textural and structural characteristics of meat. *Meat Science, 144*(January), 100–109. https://doi.org/10.1016/j.meatsci.2018.05.020

Robert, C., Bain, W. E., Craigie, C., Hicks, T. M., Loeffen, M., Fraser-Miller, S. J., & Gordon, K. C. (2023). Fusion of three spectroscopic techniques for prediction of fatty acid in processed lamb. *Meat Science, 195*, Article 109005. https://doi.org/10.1016/j.meatsci.2022.109005

Salim, A. P. A. A., Ferrari, R. G., Monteiro, M. L. G., & Mano, S. B. (2022). Effect of different feeding systems on color of longissimus muscle from Bos cattle: A systematic review and meta-analysis. *Meat Science, 192*, Article 108871. https://doi.org/10.1016/j.meatsci.2022.108871

Sandström, V., Chrysafi, A., Lamminen, M., Troell, M., Jalava, M., Piipponen, J., Siebert, S., van Hal, O., Virkki, V., & Kummu, M. (2022). Food system by-products upcycled in livestock and aquaculture feeds can increase global food supply. *Nature Food, 3*(9), 729–740. https://doi.org/10.1038/s43016-022-00589-6

Sanz, J. A., Fernandes, A. M., Barrenechea, E., Silva, S., Santos, V., Gonçalves, N., Paternain, D., Jurio, A., & Melo-Pinto, P. (2016). Lamb muscle discrimination using hyperspectral imaging: Comparison of various machine learning algorithms. *Journal of Food Engineering, 174*, 92–100. https://doi.org/10.1016/j.jfoodeng.2015.11.024

Selver, M. A., Secmen, M., & Zoral, E. Y. (2018). Savitzky-golay filtering for scattered signal de-noising. *Journal of Physics: Conference Series, 1141*, Article 012151. https://doi.org/10.1088/1742-6596/1141/1/012151

Shaikh, M. S., Jaferzadeh, K., Thörnberg, B., & Casselgren, J. (2021). Calibration of a hyper-spectral imaging system using a low-cost reference. *Sensors, 21*(11), 3738. https://doi.org/10.3390/s21113738

Silva, R. H. P., Rezende, A. S. C. de, & Inácio, D. F. da S. (2016). Pectin-rich by-products in feeding horses—a review. *Cogent Food & Agriculture, 2*(1), Article 1193925. https://doi.org/10.1080/23311932.2016.1193925

Tripathi, A. D., Mishra, R., Maurya, K. K., Singh, R. B., & Wilson, D. W. (2019). Estimates for world population and global food availability for global health. In *The role of functional food security in global health* (pp. 3–24). Elsevier. https://doi.org/10.1016/B978-0-12-813148-0.00001-3.

Tzamaloukas, O., Neofytou, M. C., & Simitzis, P. E. (2021). Application of olive by-products in livestock with emphasis on small ruminants: Implications on rumen function, growth performance, milk and meat quality. *Animals, 11*(2), 531. https://doi.org/10.3390/ani11020531

Wadhwa, M., & Bakshi, M. (2013). Utilization of fruit and vegetable wastes as livestock feed and as substrates for generation of other value-added products. http://www.fao.org/docrep/018/i3273e/i3273e.pdf.

Wan, G., Fan, S., Liu, G., He, J., Wang, W., Li, Y., Cheng, L., Ma, C., & Guo, M. (2023). Fusion of spectra and texture data of hyperspectral imaging for prediction of myoglobin content in nitrite-cured mutton. *Food Control, 144*, Article 109332. https://doi.org/10.1016/j.foodcont.2022.109332

Wang, C., Wang, S., He, X., Wu, L., Li, Y., & Guo, J. (2020). Combination of spectra and texture data of hyperspectral imaging for prediction and visualization of palmitic acid and oleic acid contents in lamb meat. *Meat Science, 169*, Article 108194. https://doi.org/10.1016/j.meatsci.2020.108194

Weng, S., Guo, B., Du, Y., Wang, M., Tang, P., & Zhao, J. (2021). Feasibility of authenticating mutton geographical origin and breed via hyperspectral imaging with effective variables of multiple features. *Food Analytical Methods, 14*(4), 834–844. https://doi.org/10.1007/s12161-020-01940-y

Williams, P., & Norris, K. H. (2001). *Near-infrared technology in the agricultural and food industries* (2nd ed.). American Association of Cereal Chemists, Inc.

Wood, J. D., Enser, M., Fisher, A. V., Nute, G. R., Sheard, P. R., Richardson, R. I., Hughes, S. I., & Whittington, F. M. (2008). Fat deposition, fatty acid composition and meat quality: A review. *Meat Science, 78*(4), 343–358. https://doi.org/10.1016/j.meatsci.2007.07.019

Wu, G., Fang, Y., Jiang, Q., Cui, M., Li, N., Ou, Y., Diao, Z., & Zhang, B. (2023). Early identification of strawberry leaves disease utilizing hyperspectral imaging combing with spectral features, multiple vegetation indices and textural features. *Computers*

and Electronics in Agriculture, 204, Article 107553. https://doi.org/10.1016/j.compag.2022.107553

Xiong, Z., Sun, D.-W., Pu, H., Zhu, Z., & Luo, M. (2015). Combination of spectra and texture data of hyperspectral imaging for differentiating between free-range and broiler chicken meats. *LWT - Food Science and Technology, 60*(2), 649–655. https://doi.org/10.1016/j.lwt.2014.10.021

Yang, D., He, D., Lu, A., Ren, D., & Wang, J. (2017). Combination of spectral and textural information of hyperspectral imaging for the prediction of the moisture content and storage time of cooked beef. *Infrared Physics & Technology, 83*, 206–216. https://doi.org/10.1016/j.infrared.2017.05.005

Yue, S., Li, P., & Hao, P. (2003). SVM classification: Its contents and challenges. *Applied Mathematics-A Journal of Chinese Universities, 18*(3), 332–342. https://doi.org/10.1007/s11766-003-0059-5

Zayed, N., & Elnemr, H. A. (2015). Statistical analysis of haralick texture features to discriminate lung abnormalities. *International Journal of Biomedical Imaging*, 1–7. https://doi.org/10.1155/2015/267807, 2015.